Viscosity of oceanic asthenosphere inferred from remote triggering of earthquakes

Fred F. Pollitz and Roland Bürgmann

Department of Geology
University of California, Davis
Davis, CA 95616
U.S.A.

Barbara Romanowicz

University of California
Seismological Laboratory
475 McCone Hall
Berkeley, CA 94720
U.S.A.

Published in
Science
May 22, 1998

A sequence of large interplate earthquakes from 1952-1965 along the Aleutian arc and Kurile-Kamchatka trench released accumulated stresses along nearly the entire northern portion of the Pacific plate boundary. The postseismic stress evolution across the northern Pacific and Arctic basins, calculated from a viscoelastic coupling model with an asthenospheric viscosity of 5×10^{17} Pa s, is consistent with triggering of oceanic intraplate earthquakes, temporal patterns in seismicity at remote plate boundaries, and space-based geodetic measurements of anomalous velocity over a 7000 by 7000 km^2 area during the 30 year period following the sequence.

Stress pulses travelling away from an earthquake source area effectively transmit the local stress changes associated with the earthquake to a much larger area as the ductile sublithospheric channel gradually yields with time (*1*,*2*,*3*,*4*). Several studies have applied such a model to the continental lithosphere, where predictions may be readily compared with geodetic observations (for example, *3*,*5*,*6*,*7*). There have also been a few applications suggestive of stress diffusion through the ocean basins (*1*,*2*,*8*). Here we evaluate postseismic stress evolution driven by large subduction events that occurred along the Aleutian and Kurile-Kamchatka trenches from 1952 to 1965 (Fig. 1**A**) and use the inferred correlation with seismicity to estimate the viscosity of the oceanic asthenosphere. The subduction earthquakes have total seismic moment exceeding 1000×10^{20} N m and are by far the largest involving the Pacific plate to have occurred during the period 1950-1970 (*9*). Moreover, each of them occurred on subduction interfaces that had experienced smaller events on timescales of 20-90 years but no comparable large ruptures for at least the past 200 years (*10*). Because these events involve only the Pacific-North America plate boundary, stress changes may be evaluated without any significant complications over the entire Pacific basin as well as the Arctic basin (on the North American plate). We specified the elastic deformation associated with these earthquakes in terms of the fault planes and slip directions shown in Fig. 1**A** and source parameters from (*11*). We also included a few smaller but significant events with total seismic moment of ~ 150×10^{20} N m: thrust events along the Kurile/Bonin arc in 1958, 1963, 1968, 1969, 1972, 1973, and 1978, and the 1986 Andreanof Islands earthquake along the Aleutian arc (*12*).

We constructed a rheology appropriate for the oceanic lithosphere from the seismic structure determined by Gaherty et al. (*13*) and then calculated postseismic gravitational-viscoelastic relaxation on a grid covering the northern Pacific and Arctic basins (*4*). The model implies that for an asthenospheric viscosity of $\eta = 5\times10^{17}$ Pa s the leading edge of the stress pulse is passing by the Juan de Fuca plate in 1975 and California in 1985 (southward propagating blue region in Fig. 1). The dispersive character of the propagating stress pulse is such that regions along the advancing front at a given time experience locally high horizontal velocities (*3*,*4*). Thus the fronts of spatially maximal strain rate and temporally maximal velocity nearly

coincide. Although the former is most useful for demonstrating the pulse-like behavior of the stress diffusion process, the latter provides a physical connection between stress diffusion within the oceanic plate and induced strains at or across adjacent plate boundaries.

Passage of the predicted velocity front is correlated with spatio-temporal patterns in western North America seismicity over the past four decades provided that asthenospheric viscosity is close to 5×10^{17} pa s. Seismic activity may be adequately represented as simply a function of time and latitude. From a suitable catalogue (*14*) spanning the time period 1963-1996 at magnitudes above $m_b = 5.3$, let $t_{eq}(i)$ and $\mathrm{lat}_{eq}(i)$ be the time of occurrence and latitude, respectively, of the ith earthquake. Similarly, let us define $\mathrm{lat}_{vel}(t)$ as the latitude of areas just adjacent to the Pacific margin off western North America that experience a velocity maximum at time t. In order to test how consistent this catalogue is with the southward progression of the velocity front we construct the correlation function in latitude–time space

$$f(\mathrm{lat},t) = \frac{1}{A(\mathrm{lat},t)} \sum_i m_b(i) \qquad (1)$$

where the summation is for events i that satisfy

$$\mathrm{lat}_{vel}(t_{eq}(i)) + \mathrm{lat} - \mathrm{lat}_{vel}(t) - 3.0^o < \mathrm{lat}_{eq}(i) < \mathrm{lat}_{vel}(t_{eq}(i)) + \mathrm{lat} - \mathrm{lat}_{vel}(t) + 3.0^o \qquad (2)$$

The inequality condition in (2) effectively sweeps out a latitude band 6° in width parallel to the $\mathrm{lat}_{vel}(t)$ versus t curve and sums the magnitude of earthquakes occurring within that band. The normalization factor $A(\mathrm{lat},t)$ is proportional to the area swept out by this band and corrects for the fact that bands near the corners of the latitude-time window are smaller than those near the middle diagonal. This correlation function enforces a strictly banded structure parallel to $\mathrm{lat}_{vel}(t)$. An alternative definition of Eq. 1 could involve either number of events or seismic moment rather than m_b, but results are similar in all cases. As shown in Fig. 2 the observed seismicity is correlated with passage of the velocity front generated by the great Aleutian and Kurile–Kamchatka events of 1952 to 1965. The structure of $f(\mathrm{lat},t)$ is asymmetric about its maximum central band, implying, if our model is correct, that passage of the front generally initiated vigorous seismic activity in a given region and seismic activity continued for a number of years. This analysis can not discriminate between continued activity triggered directly by the velocity front and secondary activity triggered by stress changes generated by the initial activity, but it does suggest that accumulated transient displacement (time integrated transient velocity) along a particular plate margin plays a significant role.

Ultimately, of course, it is accumulated stress changes which likely trigger earthquakes. At a neighboring mid-ocean ridge system such as the Juan de Fuca ridge system, lithospheric thickness shallows to less than 5 km, and partially molten material distributed in magma chambers and dikes is present. It seems likely that an increase in velocity of one of the bounding oceanic plates would lead to rapid stress concentration in the axial rift zone and subsequent

seismic or aseismic failure of the rift segments at anomalously high rates. Increased seismicity rates on short offset transform faults such as the Blanco and Mendocino fracture zones may similarly result from intense stress concentration in the weak transform fault zone compounded by loading from the more rapidly opening rift zones which bound them. Finally, near an ocean-continent boundary such as just west of the San Andreas fault (SAF), the upper crust is likely weaker than the oceanic lithosphere with which it is in contact, and the lower crust is also weak. In this case, strains induced on the continental side should depend predominantly on the local displacement of the oceanic side, although the mechanism of strain accumulation within the continental crust is uncertain.

Predicted postseismic North American plate velocity has generally been directed away from both the eastern Arctic and Juan de Fuca spreading systems in the sense promoting rifting and reached peaks in the late 1970's in both regions. If the background North America to Eurasia separation rate is prescribed by model NUVEL-1A (*15*) and postseismic velocity is presumed to represent transient North America velocity with respect to a fixed Eurasia, then the background and transient velocities may be superimposed to obtain time-dependent separation rate. The transient component is predicted to have been up to 1 cm/yr in the eastern Arctic basin, where the background component varies from 0.4 to 1.2 cm/yr. Seismicity patterns of all eastern Arctic events with $m_b \geq 5.0$ [since 1955, from which date the catalogue is believed to be complete for $m_b \geq 5.0$ (*16*)] exhibit a good correlation with the summed velocity pattern (Fig. 3**A**). Seismicity rates along the entire eastern Arctic ridge system exhibit an increase from one time period to the next, and that part of the oceanic rift system nearest the Asian continent underwent the largest velocity increase and largest increase in seismicity rate as measured by moment release.

In central California (35–39° N) the transient Pacific plate motion is predicted to have reached a maximum 2.6 mm/yr towards N40° W in 1980-1985 (parallel to the SAF), and in southern California south of the Big Bend region (32–35° N) the transient motion is predicted to have reached a maximum of 1.7 mm/yr towards N39° W in 1985-1990 (25-30° oblique to the SAF in the sense to increase compressional stress across the fault system near the Big Bend) (Fig. 3**B**). The direction of transient motion in both regions is nearly parallel to the background motion prescribed by NUVEL-1A. In northern California, the transient velocity increase, as manifested by the accumulated transient displacement, is well correlated with the observed increase in predominantly strike-slip activity. In southern California, the temporal increase in observed seismicity since the 1971 San Fernando earthquake also closely follows accumulated displacement. Although the overall seismicity rate in southern California was approximately constant from 1969 to 1992 (*17*), between latitudes 34° N and 35° N the rate of occurrence of "non-SAF" type events has been particularly high since 1986 (*18*). This

increase in non-SAF type events has been attributed (*18*) to a transient increase in the component of Pacific to North America (P-NA) relative plate velocity normal to the San Andreas fault in southern California, and our model provides a mechanism for this transient increase.

Although there may be a correlation of plate-boundary seismicity over the entire western North America margin with the predicted stress pulse propagation in the adjacent Pacific oceanic lithosphere, it does not imply a causal mechanism for every earthquake but rather a causal relationship with transient oceanic velocity in a statistical sense. Our analysis therefore suggests, but does not require, a major role for "external triggering" of California earthquakes since ~ 1979. This idea connects well with the hypothesis that northern California emerged from the stress shadow created by the 1906 San Francisco earthquake in the 1980's (*19*), making the region particularly susceptible to external triggering. The triggering of California earthquakes at a relatively high threshold ($m_b \geq 5.0–5.3$), as implied by our analysis, suggests that a transient velocity increase applied to the edge of a continental shear zone may concentrate transient stresses deep within the seismogenic layer (15–20 km depth) where larger events are typically initiated. Efforts to identify the predicted accelerations (ca. 2 mm/yr over the period 1965/1970–1980/1985) are inconclusive. Accurate space–based geodetic data have been available since 1983 in California, at which time most of the acceleration had already taken place. Repeated geodolite measurements made since the early 1970's within several southern California networks (*20*) may have potential for resolving a transient acceleration, but the small signal that we predict is likely to be at the limit of detectability of these networks.

Two intraplate oceanic earthquakes may have potentially been triggered by the postseismic stress diffusion. These are the m_b=5.5 April 28, 1968 event in the northern Pacific basin, which has a thrust mechanism (*21*), and the m_b=6.8 February 21, 1991 Bering Sea earthquake, characterized as a combined strike-slip and rifting event (*22*). We find that each event is located in a region where local strain rates in the sense promoting triggering were strong at their time of occurrence (Fig. 3**C**). The accumulated postseismic stress change σ_{xx} is calculated at 0.3 bars and 0.8 bars for the 1968 and 1991 events, respectively. Such a stress change is often sufficient to trigger comparable continental seismicity (*23*), especially considering that the respective source areas were likely pre-existing zones of weakness (*22*,*24*).

The correlations with the oceanic intraplate events in Fig. 3**C** are found to break down for $\eta < 3 \times 10^{17}$ Pa s, while $\eta > 8 \times 10^{17}$ Pa s still produces correlations but involves stress changes one order of magnitude lower. The obtained correlations with western North America seismicity imply that if $\eta = 8 \times 10^{17}$ Pa s then most of the acceleration in seismic activity would take place long before passage of the velocity front, and if $\eta = 3 \times 10^{17}$ Pa s most seismic activity would occur long after it; the notion that transient rates are relatively high for $\eta = 3 \times 10^{17}$ Pa s would further aggravate this problem. A similar argument applies to east

Arctic ridge seismicity. Finally, to produce the same diffusion behavior with a thicker lithosphere would require greater asthenospheric viscosity. Given our choice for the lithospheric thickness, our preferred value is $\eta = 5 \times 10^{17}$ Pa s, which is compatible with the data in the Arctic and north Pacific basins. The overall viscosity structure we infer (*13*) agrees well with the viscosity structure beneath a mid–ocean ridge based on the physical properties of wet olivine aggregates(*25*). Our results imply that the evolution of off–ridge–axis oceanic mantle preserves the essential features of the ridge–axis viscosity structure. Small–scale convection, which may act to "flatten" age–depth and age–heat flow relationships for the oceanic lithosphere(*26*), may produce a similar flattening of the off–ridge viscosity structure.

Detectable transient velocities are predicted even very far (~ 4000 km) from the Aleutian trench in the mid-Pacific, where Global Positioning System (GPS) and Very Long Baseline Interferometry (VLBI) data can be evaluated. Fig. 4**A** shows P-NA anomalous horizontal velocity at several Pacific geodetic sites, with relative motion model NUVEL-1A serving as the reference model (*27*). The predictions of the viscoelastic coupling model are superimposed. The general agreement between the internal Pacific strain patterns prescribed by our model and the geodetic observations is best demonstrated by referring the anomalous velocities obtained in Fig. 4**A** to a different P-NA angular velocity vector $\boldsymbol{\omega}$ which we derive (*28*). The anomalous velocities relative to the derived $\boldsymbol{\omega}$ are shown in Fig. 4**B**. An objective measure of the internal deformation of the Pacific plate based on these geodetic measurements is

$$\sigma^2 = \frac{1}{12} \sum_{i=1}^{12} (\gamma_i)^2 + (\beta_i)^2 \qquad (3)$$

where $\{\gamma_i\}$ and $\{\beta_i\}$ represent the set of all angle changes and relative arc length changes among all four spherical triangles which can be constructed from the four mid-Pacific geodetic sites. This measure is invariant with respect to a rigid rotation of the velocity field and contains information on mean shear strain and dilatation within this broad network. The mean observed σ^2 is 1.06 $(10^{-9}$ rad$)^2$, and after correction for transient velocities this measure decreases to 0.27 $(10^{-9}$ rad$)^2$; that is, a reduction of 75%. A numerical perturbation simulation using the error distribution of the data shows that the probability that this reduction could be explained with observation error alone is 0.7% (Fig. 4**C**).

Although geodetic observations made near plate boundaries are often acknowledged as being susceptible to the transient effects of earthquakes, our analysis suggests that even areas well within a plate interior may be susceptible to significant and tangible transient effects from plate boundary earthquakes. Our model makes concrete predictions regarding transient Pacific plate velocity which are testable with present and future space-based geodetic data. From the results obtained here it appears likely that the Pacific lithosphere has been subjected to substantial spatially and temporally varying velocity fluctuations over the past four decades, and the

assumption of rigid behavior of the oceanic lithosphere which has been so successful in explaining global plate motions averaged over very long time periods may be of questionable validity on a timescale of years to decades.

References and Notes

1. W. M. Elsasser, in *The Application of Modern Physics to the Earth and Planetary Interiors,* S.K. Runcorn, Ed. (John Wiley, New York, NY, 1969), pp. 223-246.
2. D. L. Anderson, *Science* **187**, 1077 (1975).
3. P. A. Rydelek and I. S. Sacks, *Geophys. J. Inter.* **100**, 39 (1990); S. C. Cohen, *J. Geophys. Res.* **97**, 15395 (1992).
4. F. F. Pollitz, *J. Geophys. Res.* **102**, 17921 (1997).
5. P. A. Rydelek, and I. S. Sacks, *Nature, 336*, 234 (1988).
6. C. O. Sanders, *Science* **260**, 973 (1993).
7. W. Thatcher, T. Matsuda, T. Kato, and J. B. Rundle, *J. Geophys. Res.* **85**, 6429 (1980); K. Miyashita, *J. Phys. Earth* **35**, 449 (1987); T. Tabei, *J. Phys. Earth* **37**, 101 (1989); F. F. Pollitz, and I. S. Sacks, *J. Phys. Earth* **42**, 1 (1994); A. Piersanti, G. Spada, and R. Sabadini, *J. Geophys. Res.* **102**, 477 (1997).
8. J. C. Savage, *J. Geophys. Res.,* **76**, 1954 (1971); H. J. Melosh, *J. Geophys. Res.* **81**, 5621 (1976); E. Berg, G. H. Sutton, and D. A. Walker, *Tectonophysics* **39**, 559 (1977); B. Romanowicz, *Science* **260**, 1923 (1993).
9. Although the 1960 Chilean earthquake is larger than all of these events combined, the presence of the East Pacific Rise as the Pacific-Nazca plate boundary is likely to decouple its effects from the surrounding Pacific basin.
10. S. P. Nishenko, and K. H. Jacob, *J. Geophys. Res.* **95**, 2511 (1990); C. G. Bufe, S. P. Nishenko, and D. J. Varnes, *Pure Appl. Geophys.* **142**, 83 (1994).
11. F. T. Wu, and H. Kanamori, *J. Geophys. Res.* **78**, 6082 (1973); H. Kanamori, *Phys. Earth Planet. Int.* **11**, 216 (1976); S. L. Beck, and D. H. Christensen, *J. Geophys. Res.* **96**, 2205 (1991); D. H. Christensen, and S. L. Beck, *Pure Appl. Geophys.* **142**, 29 (1994); S. R. Holdahl, and J. Sauber, *Pure Appl. Geophys.* **142**, 54 (1994). Both the 1957 and 1964 rupture zones are divided into two fault planes in order to more accurately represent their overall ruptures. Assignment of uniform moment tensor density on each fault plane is adequate for the intended application.
12. H. Kanamori, *J. Geophys. Res.* **75**, 5011 (1970); H. Kanamori, *Tectonophysics* **12**, 1 (1971); K. Abe, *Phys. Earth Planet. Inter.* **7**, 143 (1973); K. Shimazaki, *Phys. Earth Planet. Inter.* **9**, 314 (1974); Y. Fukao and M. Furumoto, *Geophys. J. Roy. Astr. Soc.* **57**, 23 (1979); T. Seno et al., *Phys. Earth Planet. Inter.* **23**, 39 (1980); D. Giardini, A.

Dziewonski, and J. Woodhouse, *Phys. Earth Planet. Inter.* **40**, 259 (1985); T. M. Boyd, and J. L. Nabelek, *Bull. Seimol. Soc. Am.* **78**, 1653 (1988). A seismic moment of 10×10^{20} N m was assigned to the 1986 Andreanof Islands earthquake.

13. J. B. Gaherty, T. H. Jordan, and L. S. Gee, *J. Geophys. Res.* **101**, 22,291 (1996). The rheological structure of the oceanic lithosphere and underlying mantle is prescribed by
Layer 1 (0-8 km depth): $\lambda = \mu = 35$ GPa, $\rho = 2900$ kg-m^{-3} (purely elastic)
Layer 2 (8-62 km depth): $\lambda = \mu = 65$ GPa, $\rho = 3400$ kg-m^{-3} (purely elastic)
Layer 3 (62-213 km depth): $\lambda = \mu = 75$ GPa, $\rho = 3400$ kg-m^{-3}, viscosity=η (viscoelastic asthenosphere)
Layer 4 (below 213 km depth): $\lambda = \mu = 75$ GPa, $\rho = 3400$ kg-m^{-3}, viscosity=$1000\times\eta$
A Maxwell rheology is taken for the asthenosphere, conforming to deformation of olivine in the diffusion creep regime [S.-I. Karato, D. C. Rubie, and H. Yan, *J. Geophys. Res.* **98**, 9761 (1993)]. The total thickness of the elastic oceanic lithosphere of 62 km is only slightly smaller than the 68 km estimate of the depth to the mid-Pacific low velocity zone defined by a sharp boundary [Gaherty et al., 1996], and it is about twice as large as the effective elastic plate thickness of the oceanic lithosphere based on observations of flexure [A. B. Watts, J. H. Bodine, and N. M. Ribe, *Nature* **283**, 532 (1980); M. K. McNutt and H. W. Menard, *Geophys. J. Roy. Astr. Soc.* **71**, 363 (1982)]. Although the base of the asthenosphere is not well defined seismically, a large viscosity increase probably occurs at 200-250 km depth because of the pressure dependence of the viscosity of olivine [Karato et al. (1993)].
14. U.S.G.S. National Earthquake Information Center Catalogue.
15. C. DeMets, R. Gordon, D. Argus, and S. Stein, *Geophys. Res. Lett.* **21**, 2191 (1994).
16. J. H. Hodgeson et al., *Ann. Int. Geophys. Year* **30**, 33 (1965); K. Fujita, D.B. Cook, H. Hasegawa, D. Forsyth, and R. Wetmiller, in *The Decade of North American Geology, vol. L,* L. Grantz, L. Johnson, and J.F. Sweeney, Eds. (Geol. Soc. Am., Boulder, CO, 1990), pp. 79-100.
17. L. K. Hutton and L. M. Jones, *Bull. Seism. Soc. Am.* **83**, 313 (1993); L. M. Jones, and E. Hauksson, *Geophys. Res. Lett.* **24**, 469 (1997).
18. F. Press, and C. Allen, *J. Geophys. Res.* **100**, 6421 (1995).
19. S. C. Jaume, and L. R. Sykes, *J. Geophys. Res.* **101**, 765 (1996). The Queen Charlotte and Fairweather faults, by contrast, were subjected to ~ 10 times higher transient velocity of the adjacent oceanic lithosphere than California, but they exhibited far less triggered seismicity (Fig. 2). Large earthquakes on these faults (M8.1 in 1949 and M7.9 in 1958) created a stress shadow which has enveloped the fault system ever since, except for a gap which was filled by the 1972 Sitka earthquake [M. M. Schell and L. J. Ruff, *Phys. Earth*

Planet. Int. **54**, 241 (1989)].

20. J. C. Savage, *J. Geophys. Res.* **100**, 12691 (1995).
21. L.R. Sykes, and M.L. Sbar, in *Geodynamics of Iceland and the North Atlantic*, L. Kristjansson, Ed. (D. Reidel, Dordrecht-Holland, 1974), pp.207-224.
22. G. A. Abers, G. Ekstrom, M. S. Marlow, and E. L. Geist, *J. Geophys. Res.* **98**, 2155 (1993). Most of the cumulative stress change evaluated in the Bering Sea arises from the 1957 event in our model (contribution of 1957 event to σ_{xx} is 0.77 bars, contribution of 1986 event is 0.04 bars), but nearly all of the strain rate predicted in 1991 arises from the 1986 Andreanof Islands earthquake.
23. G. C. King, R. S. Stein, and J. Lin, *Bull. Seism. Soc. Am.* **84**, 935 (1994).
24. E. A. Bergman, and S. C. Solomon, *J. Geophys. Res.* **85**, 5389 (1980).
25. G. Hirth and D. L. Kohlstedt, *Earth Planet. Sci. Lett.* **144**, 93 (1996). Our preferred viscosity value also lies within the range 4×10^{17} to 3×10^{18} Pa s determined from thermal constraints on small scale convection [A. Davaille and C. Jaupart, *J. Geophys. Res.* **99**, 19853 (1994)].
26. B. Parsons and J. G. Sclater, *J. Geophys. Res.*, **82**, 803 (1977); C.A. Stein and S. Stein, *Nature*, **359**, 123 (1992).
27. The geodetic data consists of GPS data [K. Larson, personal communication] at KOKB on Hawaii and PAMA on Pamatai plus VLBI data [publicly available at http://lupus.gsfc.nasa.gov/vlbi.html (1996)] at KWAJAL26, MARCUS, and three Hawaiian sites. The three VLBI observations at Hawaiian sites have been averaged into a single observation. We define stable North America for the GPS data set by minimizing velocity at those seven North American GPS sites considered stable by Larson et al. [K. Larson, J. T. Freymuller, and S. Philipsen, *J. Geophys. Res.* **102**, 9961 (1997)]. A similar procedure is applied seperately to the VLBI data set.
28. We perform an inversion for the best-fitting P–NA angular velocity vector $\boldsymbol{\omega}$ using transform azimuth data from the Gulf of California [C. DeMets, R.G. Gordon, D. F. Argus, and S. Stein, *Geophys. J. Int.* **101**, 425 (1990)], the recently revised Gulf of California spreading rate of 5.1 cm/yr [C. DeMets, *Geophys. Res. Lett.* **22**, 3545 (1995)], and the geodetic observations shown in Fig. 4**A**. The newly derived $\boldsymbol{\omega}$ (52.1° S, 100.0° E, 0.79° /Myr) predicts Gulf of California spreading rates of 5.1 cm/yr and fits the Gulf of California transform azimuths equally well as model NUVEL-1A.
29. Fault parameters of the various fault planes representing these events are as follows:
    November 4, 1952: $\delta = 30°$, $h_2 = 40$ km, $h_1 = 5$ km,
    March 9, 1957: (eastern+western planes) $\delta = 18°$, $h_2 = 35$ km, $h_1 = 5$ km,
    March 28, 1964: (shallow plane) $\delta = 5.7°$, $h_2 = 20$ km, $h_1 = 5$ km,

(deeper plane) $\delta = 11.3°$, $h_2 = 35$ km, $h_1 = 20$ km,

January 24, 1965: $\delta = 18°$, $h_2 = 35$ km, $h_1 = 5$ km.

where δ is dip and h_2 and h_1 are the depth of the lower and upper fault edges, respectively. The two planes chosen for the 1957 event fill in an 880 km long section of the Aleutian arc corresponding to the total aftershock area compiled by (*30*) but excluding the easternmost aftershock activity. In choosing this fault length, which involves extending coseismic rupture considerably eastward of the limit of main-shock deformation (*31*), we suppose that the total static offset associated with such a large event is defined by the main shock plus the significant aftershocks, which may involve a considerable amount of aseismic slip. Given the large aftershock area, we scale M_0 for the 1957 earthquake up relative to that determined by (*31*) in order to reflect the greater effective fault length.

30. T. M. Boyd, E. R. Engdahl, and W. Spence, *J. Geophys. Res.* **100**, 621 (1995).
31. J. M. Johnson et al., *Pure Appl. Geophys.* **142**, 3 (1994).
32. L. R. Sykes, *Bull. Seism. Soc. Am.* **55**, 501 (1965); L. A. Savostin and A. M. Karasik, *Tectonophysics* **74**, 111 (1981); J. P. Jemsek, E. A. Bergman, J. L. Nabelek, and S. C. Solomon, *J. Geophys. Res.* **91**, 13,993. (1986); Harvard Centroid Moment Tensor Catalogue.
33. T. C. Hanks and H. Kanamori, *J. Geophys. Res.* **84**, 2348 (1979).
34. F. F. Pollitz and I. S. Sacks, *J. Geophys. Res.* **101**, 17771 (1996).
35. This work was supported by the Cooperative UC/Los Alamos Research program and a Presidential Young Investigators award to L. Kellogg. We thank K. Larson for recomputing GPS velocities, D. Argus and J. Melosh for discussions, J. Savage for a critical review, and S. Sacks and P. Rydelek for helpful comments. This research has made use of NASA Goddard Space Flight Center's VLBI terrestrial reference frame solution number 1033a3.

FIGURE CAPTIONS

Fig. 1. (**A**) Rupture areas of major subduction events along the Aleutian arc and Kamchatka trench from 1952 to 1965. Arrows give the direction of slip associated with each of the four events considered, with length proportional to total seismic moment. Numerals adjacent to these arrows specify the seismic moment in units of 10^{20} N m (*29*). (**B-D**) Net postseismic velocity and dilatational strain rate $\dot{e}_{EE}+\dot{e}_{NN}$ over the northern Pacific and eastern Arctic basins driven by combined subduction events projected onto a sphere centered on 50° N, 155° W as evaluated at three different times. Deformation is evaluated at Earth's surface. Heavy lines denote the fault planes used to model the subduction events. Locally large velocities near the rupture zones have been truncated at a maximum of 5 cm/yr for visual simplicity.

Fig. 2. Observed western North America seismicity from 1963-1995 is represented in terms of location (latitude), time t, and body wave magnitude m_b as given by the size of the circles. Correlation function $f(\text{lat},t)$ (equation 1) is obtained with either the observed or a constructed random seismicity catalogue. In the latter case, the structure of the observed seismicity is altered such that $\text{lat}_{eq}(i)$ is unchanged while $t_{eq}(i)$ becomes a random function of time obeying the uniform distribution between the years 1963 and 1995. The shape of the velocity front $\text{lat}_{vel}(t)$ for $\eta =$ 3, 5, or 8×10^{17} Pa s is indicated. Almost all seismic events used (restricted to boxed region of Fig. 1**B**) are associated with the active eastern Pacific margin. AT=Aleutian Trench, FF=Fairweather Fault, JdF=Juan de Fuca plate, MFZ=Mendocino Fracture Zone, QCT=Queen Charlottte Transform Fault, SAF=San Andreas Fault.

Fig. 3. (**A**) Epicenters of all shallow (< 30 km) $m_b \geq 5.0$ earthquakes in the eastern Arctic basin in various time periods compiled from various sources (*16*,*32*). The orientation of the tension axis is displayed where a focal mechanism solution is available. Heavy arrows plotted for 1955-1963 indicate background North America to fixed Eurasia plate motion (*15*), dashed and solid arrows for 1964-1979 indicate the background plus transient (postseismic) relative plate motion evaluated in 1967 and 1975, respectively, and the solid arrows for 1980-1994 indicate the background plus transient relative plate motion evaluated in 1985. East Arctic ridge separating North American and Eurasian plates is indicated by the dashed lines.
(**B**) Equivalent magnitude M of summed seismic moment M_0 within binned 5-year intervals in northern California (latitudes 35–39° N) and southern California (32–35° N), derived from all regional earthquakes within boxed region of Fig. 1**B** of magnitude ≥ 5.0 (*14*) and the averaged seismic moment formula of (*33*). Time-dependent transient velocity and displacement of the adjacent Pacific margin lithosphere is superimposed.
(**C**) Geographic distribution of net postseismic strain rate $\dot{e}_{xx}$ in the vicinity of the m_b=5.5 April 28, 1968 and the m_b=6.8 February 21, 1991 Bering Sea earthquakes, where x is oriented parallel to either the pressure axis with azimuth N77° E (1968 event) or the tension axis with azimuth S2° W (1991 event).

Fig. 4. (**A**) Anomalous GPS (light arrows) and VLBI (heavy arrows) velocities with respect to the P–NA velocity predicted from model NUVEL-1A. VLBI velocity plotted at KOKB has been averaged over three Hawaiian VLBI sites. These anomalous velocities have been derived from GPS and VLBI velocities at Pacific and selected North American sites. Observed anomalous velocities are shown with the corresponding 1–σ error ellipses. Dashed arrows show the transient velocity predicted from our viscoelastic coupling model. Observations and predictions correspond to the time periods 1984-1988 (VLBI site KWAJAL26), 1988-1992 (VLBI site MARCUS), 1991-1997 (GPS site KOKB), 1992-1997 (GPS site PAMA) and 1984/1993-1996 (VLBI Hawaiian sites). (**B**) Anomalous GPS and VLBI velocities with respect to the velocity predicted from our derived P–NA angular velocity vector. Agreement with VLBI data alone is excellent, and GPS velocity estimates at Hawaii have diverged markedly from VLBI estimates since 1995 for unknown reasons. (**C**) Distribution of σ^2 (equation 3) represented as a histogram of simulated σ^2 in bins of 0.07 $(10^{-9}\text{rad / yr})^2$. The simulation

consists of 10000 realizations of a data perturbation procedure described by (*34*) designed to test the likelihood that the low σ^2 obtained after accounting for our calculated transient effects could be due to chance. The σ^2 calculated directly from the observed data and the residual value calculated after correcting the data for our modeled transient velocities are indicated by vertical arrows. The area of the histogram to the right of the residual arrow is only 0.7% of the total area.

Figure 1

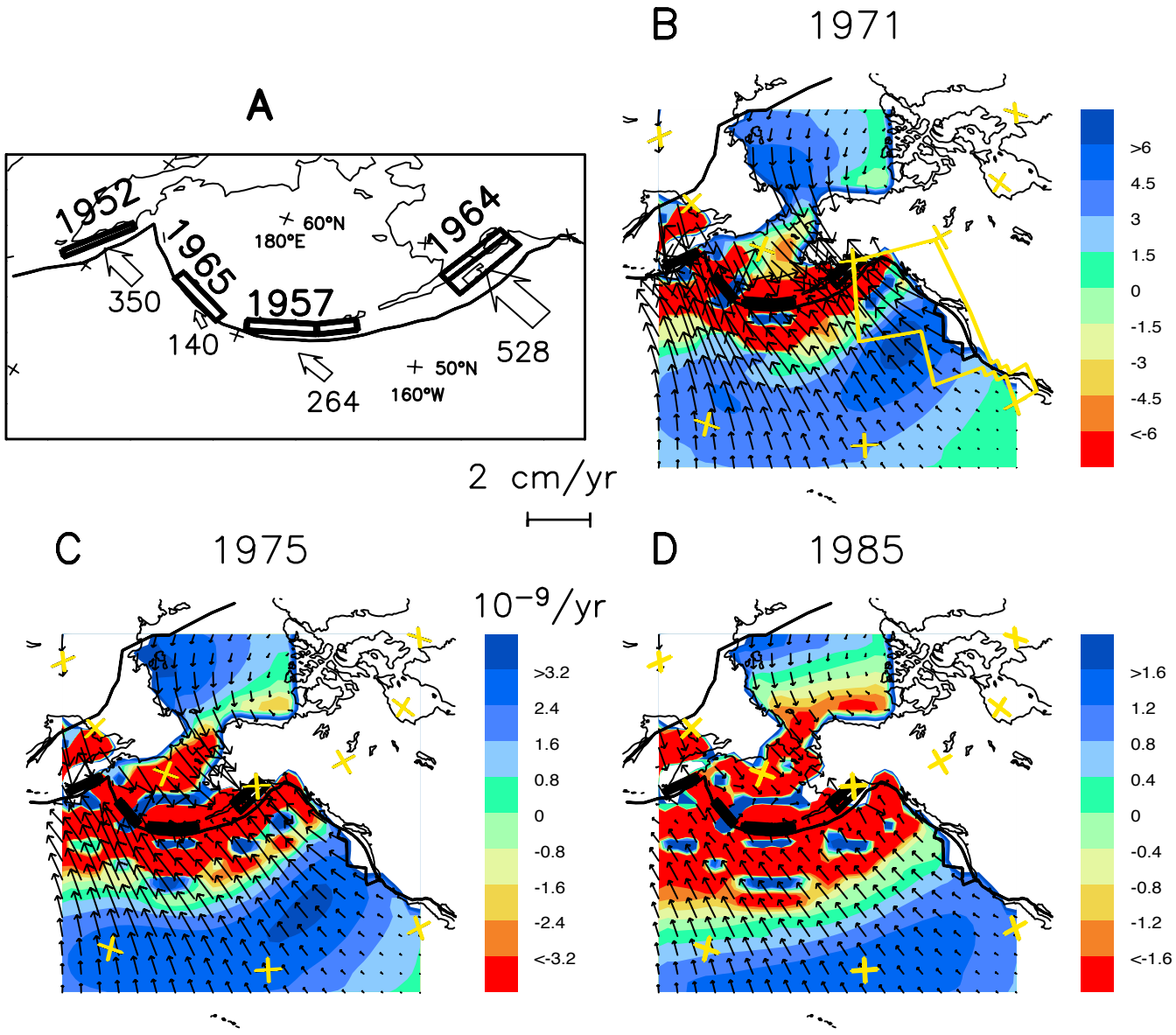
A
1952
1965
1957
1964
60°N
180°E
350
140
264
528
50°N
160°W
B
1971
>6
4.5
3
1.5
0
-1.5
-3
-4.5
<-6
2 cm/yr
C
1975
>3.2
2.4
1.6
0.8
0
-0.8
-1.6
-2.4
<-3.2
10⁻⁹/yr
D
1985
>1.6
1.2
0.8
0.4
0
-0.4
-0.8
-1.2
<-1.6

Figure 2

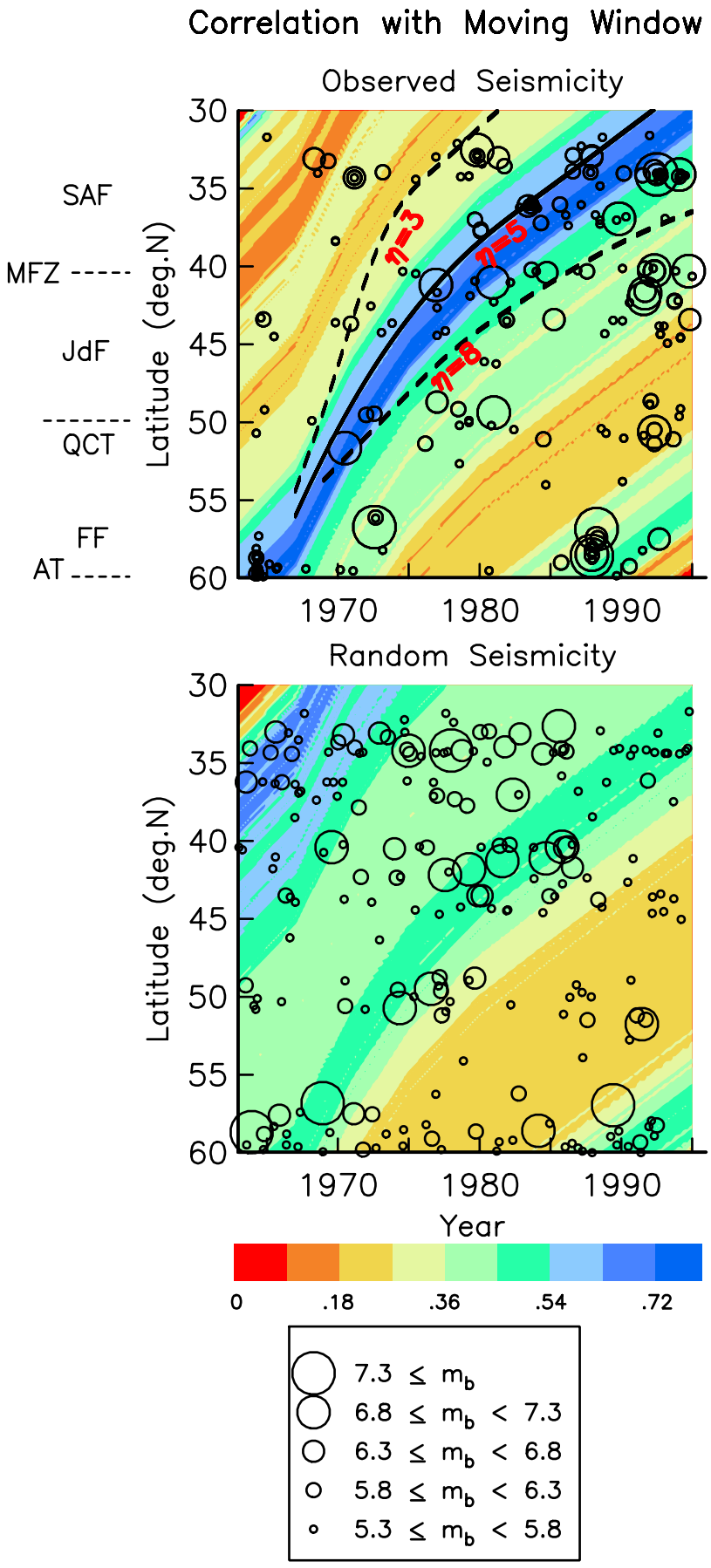
Correlation with Moving Window
Observed Seismicity
SAF
MFZ
JdF
QCT
FF
AT
Latitude (deg.N)
30
35
40
45
50
55
60
η=3
η=5
η=8
1970
1980
1990
Random Seismicity
Year
0
.18
.36
.54
.72
7.3 ≤ m_b
6.8 ≤ m_b < 7.3
6.3 ≤ m_b < 6.8
5.8 ≤ m_b < 6.3
5.3 ≤ m_b < 5.8

Figure 3

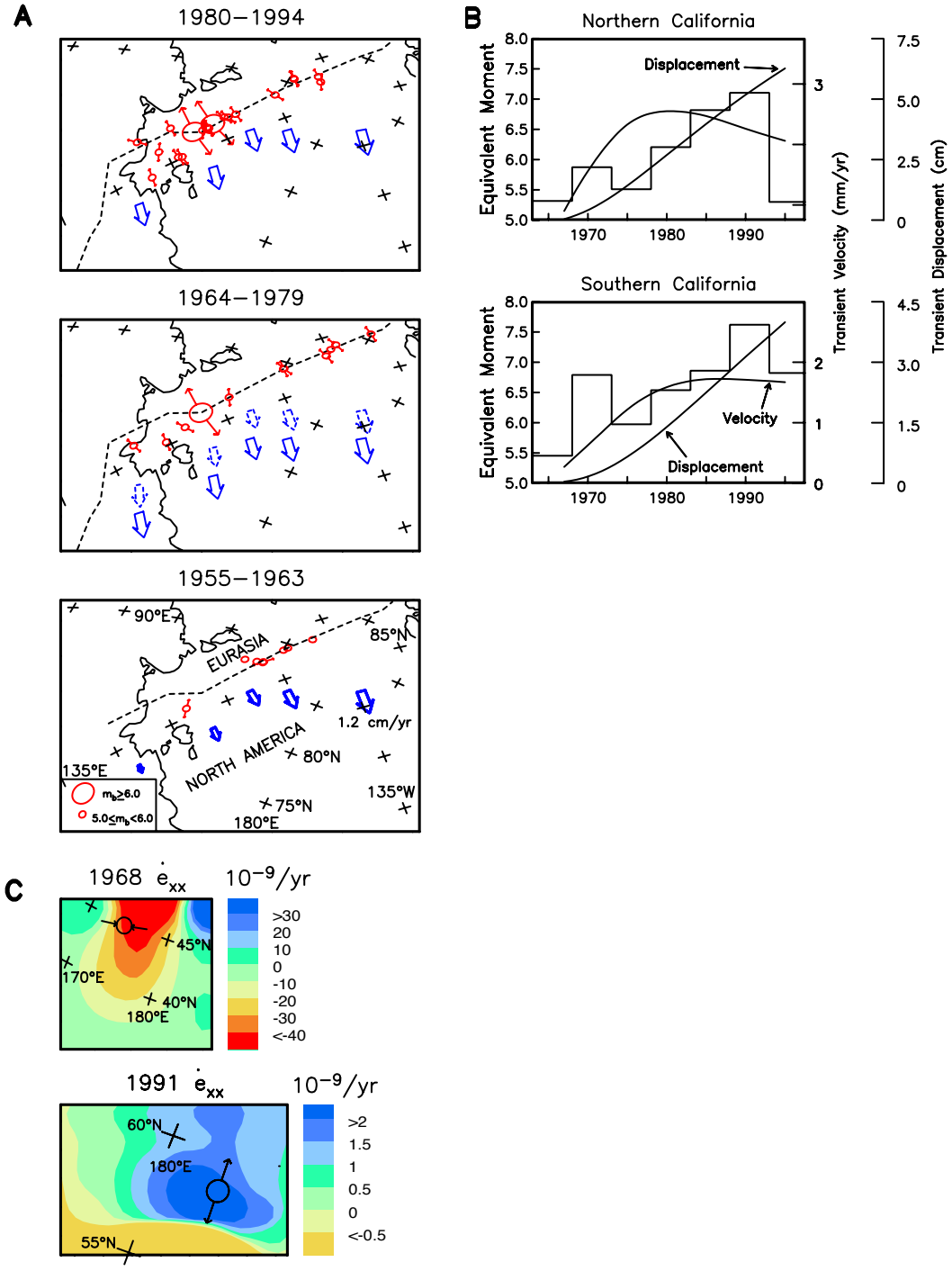
A
1980–1994
1964–1979
1955–1963
90°E
EURASIA
85°N
1.2 cm/yr
NORTH AMERICA
80°N
135°E
135°W
75°N
180°E
$m_b \geq 6.0$
$5.0 \leq m_b < 6.0$
B
Northern California
Displacement
Equivalent Moment
Transient Velocity (mm/yr)
Transient Displacement (cm)
1970
1980
1990
Southern California
Velocity
Displacement
C
1968 $\dot{e}_{xx}$ 10^{-9}/yr
>30
20
10
0
-10
-20
-30
<-40
45°N
170°E
40°N
180°E
1991 $\dot{e}_{xx}$ 10^{-9}/yr
>2
1.5
1
0.5
0
<-0.5
60°N
180°E
55°N

Figure 4

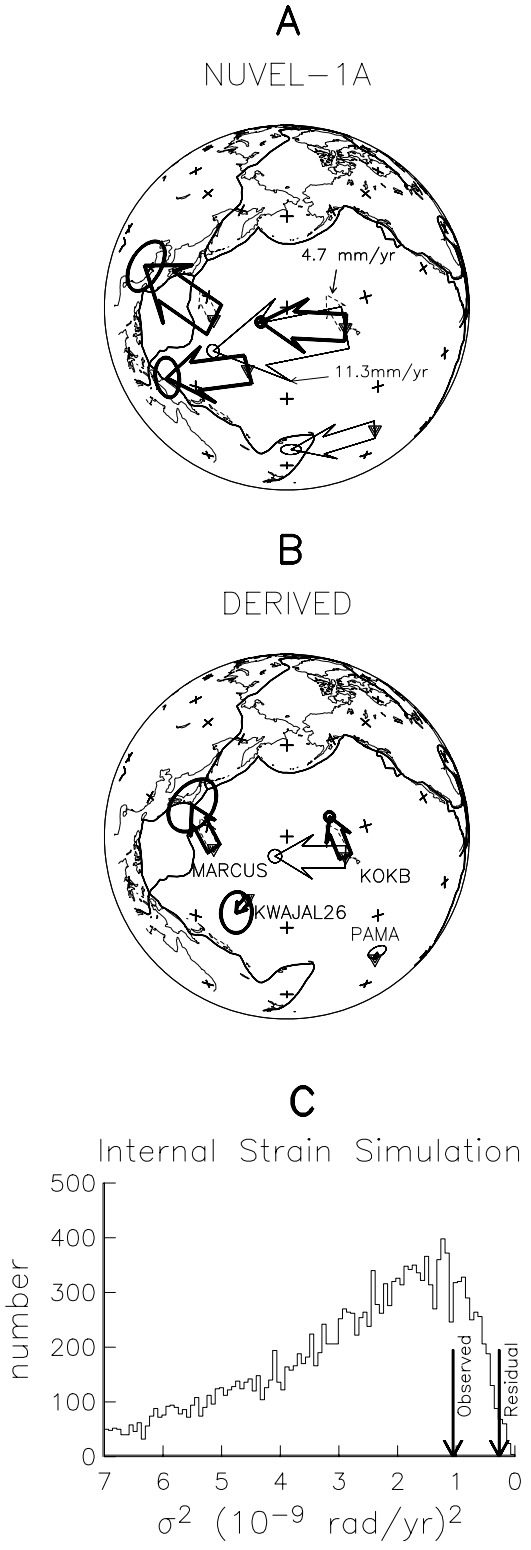
A
NUVEL−1A
4.7 mm/yr
11.3mm/yr
B
DERIVED
MARCUS
KOKB
KWAJAL26
PAMA
C
Internal Strain Simulation
number
500
400
300
200
100
0
7
6
5
4
3
2
1
0
Observed
Residual
σ2 (10−9 rad/yr)2